



Impacts of atmospheric and oceanic factors on monthly and interannual variations of polynya in the East Siberian Sea and Chukchi Sea

ZHANG Yu^{a,b,c}, ZHANG Yan-Yan^a, XU Dan-Ya^{b,*}, CHEN Chang-Sheng^d, SHEN Xin-Yi^a, HU Song^{a,c}, CHANG Liang^{a,c}, ZHOU Xiang-Qian^e, FENG Gui-Ping^{a,c}

^a College of Marine Sciences, Shanghai Ocean University, Shanghai, 201306, China

^b Southern Marine Science and Engineering Guangdong Laboratory (Zhuhai), Zhuhai, 519082, China

^c International Center for Marine Studies, Shanghai Ocean University, Shanghai, 201306, China

^d School for Marine Science and Technology, University of Massachusetts-Dartmouth, New Bedford, MA, 02744, USA

^e State Key Laboratory of Estuarine and Coastal Research, East China Normal University, Shanghai, 200241, China

Received 10 October 2020; revised 21 April 2021; accepted 8 July 2021

Available online 21 July 2021

Abstract

As a key region of Northeast Passage, the polynya along the Siberian coast in the East Siberian and Chukchi Seas is important to local dynamic and thermodynamic processes, sea ice production and marine ecosystem. The detailed variations of polynya and the contributions of atmospheric and oceanic factors to the polynya have not been explored quantitatively. AMSR-E satellite data from January to April during the period 2003–2011 were used to study the impacts of wind stress and ocean heat transport on variations of polynya in the East Siberian Sea and Chukchi Sea. The study region was divided into six domains. Four sets of AMSR-E data with resolutions of 6.25 km and 12.5 km were compared based on two algorithms of sea ice concentration (referred to as 6.25 km-IC and 12.5 km-IC) and sea ice thickness (referred to as 6.25 km-h and 12.5 km-h). The monthly and yearly polynya areas in the four cases and six domains had remarkable differences. The two cases of 6.25 km-h and 12.5 km-h had larger areas of polynya than the other two cases of 6.25 km-IC and 12.5 km-IC. The difference in polynya area between the 6.25 km-h and 12.5 km-h cases was much smaller than the difference between the 6.25 km-IC and 12.5 km-IC cases. The study of atmospheric and oceanic mechanisms on polynya is influenced significantly by the sensitivity of polynya areas. In general, the impact of wind stress and ocean heat transport on the polynyas had noticeable monthly and interannual variations and was dependent on the locations of the polynyas. The alongshore and offshore wind had stronger correlations with the polynya area than ocean heat transport. Although the higher resolution (6.25 km) AMSR-E data are best for the study of atmospheric and oceanic impacts on polynya area, the coarse resolution (12.5 km) AMSR-E data based on sea ice thickness can also be used. Wind direction dominated the polynya area in the East Siberian Sea and wind speed dominated the polynya area in the Chukchi Sea. The variation in ocean heat transport was influenced mainly by variation in volume transport rather than variation in water temperature.

Keywords: Polynya area; AMSR-E; Wind; Ocean heat transport

1. Introduction

Sea ice in the Arctic Ocean has a significant impact on both basin and local scale ocean processes, including the radiation balance due to high ice-albedo feedback (Hall, 2004; Perovich et al., 2007), heat transport due to ice insulating properties (Maykut and McPhee, 1995; Lytle and Ackley, 1996; Sturm et al., 2002; Screen and Simmonds, 2010), and freshwater

* Corresponding author.

E-mail address: xudanya@sml-zhuhai.cn (XU D.-Y.).

Peer review under responsibility of National Climate Center (China Meteorological Administration).

change due to ice formation and melt (Häkkinen, 1993; McPhee et al., 1998; Yamamoto-Kawai et al., 2008). Sea ice cover in the Arctic Ocean has very strong seasonal variability (Johannessen et al., 2004) with the minima in September and the maxima in March. In general, the sea ice cover in the central Arctic Ocean persists throughout the year. However, the coastal regions have very different characteristics. Since the late 1970s, dramatic Arctic warming has caused rapid sea ice retreat (Bi et al., 2020; Comiso, 2006, 2012; Stroeve et al., 2007) and sea ice thinning (Kwok and Rothrock, 2009; Kwok et al., 2009; Liang and Losch, 2018; Rothrock et al., 1999) in coastal areas.

The Siberian coast is a key region in the Arctic Ocean for ship navigation through the Northeast Passage (Lei et al., 2015). A wide continental shelf exists in the East Siberian Sea and Chukchi Sea. During winter and spring, these two seas are covered with sea ice. However, in the coastal regions of the East Siberian Sea and the Chukchi Sea, a number of polynyas (open water areas surrounded by ice) have occurred between January and April. These polynyas could improve the possibility of shipping through the Northeast Passage. Polynyas, which occur at freezing temperatures (Barber et al., 2001), play a significant role in thermal dynamics, local ocean circulation, sea ice production, and the overall marine ecosystem. Polynyas have a positive effect on atmospheric mesoscale motion by releasing heat from the ocean to the atmosphere at a rate one to two orders of magnitude greater than occurs with thick ice (Maykut, 1982; Kottmeier and Engelbart, (1992)). The brine rejection and ocean surface cooling in polynyas lead to vertical mixing and convection, contributing to the transformation of intermediate and deep waters and maintenance of the oceanic overturning circulation (Morales Maqueda et al., 2004). During the formation of polynyas, the low temperature and high salinity water produced by freezing and brine rejection is an important source of polar water masses (Schauer, 1995). Polynyas also provide the appropriate environment for marine animals and plants (Grebmeier and Cooper, (1995)).

The Arctic polynyas are influenced by atmospheric and oceanic factors. In general, polynyas can be divided into sensible heat polynyas and latent heat polynyas. Sensible heat polynyas are controlled by oceanic thermodynamics that melt existing sea ice and prevent new sea ice formation (Melling et al., 2015). Latent heat polynyas are driven by atmospheric and oceanic dynamics, including winds and ocean currents, which produce divergent sea ice motion (Morales Maqueda et al., 2004). Most of the Arctic polynyas are thought to be latent heat polynyas, but many shelf water polynyas are considered to be hybrid polynyas maintained by both sensible heat and wind forcing (Kozo, 1991; Hirano et al., 2016; Ladd et al., 2016). Fukamachi et al. (2017) suggested that strong offshore wind and upwelling of Atlantic Water could contribute to the formation of polynyas in the northeastern Chukchi Sea. Pisareva et al. (2019) arrived at a similar conclusion that the Northeast Chukchi Polynya was affected by both wind and upwelled warm water. In their study of the Bering Sea, Durski and Kurapov (2020) determined that wind

was correlated with the polynyas. Vincent (2019; 2020) found that the maintenance of the North Water Polynya in the region of Nares Strait was caused by southward ice advection under the combined effect of wind, tide and ocean currents.

Over the East Siberian Sea and Chukchi Sea, the wind is controlled by the combined effects of the Siberian and Beaufort Highs and Aleutian Low (Danielson et al., 2014). The variability of atmospheric pressure also influences the current field in the region. In general, the northward Pacific inflow enters the Chukchi Sea and separates into three main branches (Woodgate et al., 2005). An eastward Siberian Coastal Current runs over the shelf from the East Siberian Sea to the Chukchi Sea (Semiletov et al., 2005). Owing to the harsh environment in the polar region, *in situ* observations of polynyas are very limited. Currently, research on Arctic polynyas has been based on remote sensing data. Specific studies focused on polynyas in the East Siberian Sea and Chukchi Sea are still few. Martin and Cavalieri (1989) suggested that the Siberian shelf polynyas form 20%–60 % of the Arctic intermediate water. Winsor and Björk (2000) determined that the polynya in the Chukchi Sea was one of the regions with largest sea ice production in the Arctic Ocean. Ingram et al. (2002) found that oceanic heat transport contributed to the presence of polynyas. In the Chukchi Sea, winds and ocean currents might contribute equally to the formation of polynyas (Morales Maqueda et al., 2004). The northernmost part of the Chukchi Polynya is thought to contain combined sensible and latent heat polynya driven by wind stress (Hirano et al., 2016).

Satellite data have limitations. The remote sensing data used for the study of Arctic polynyas include Aqua Advanced Microwave Scanning Radiometer-E (AMSR-E), Advanced Land Observing System (ALOS), Synthetic Aperture Radar (SAR), Moderate-resolution Imaging Spectroradiometer (MODIS), Advanced Very High Resolution Radiometer (AVHRR), and Special Sensor Microwave/Imager (SSM/I). Since both the MODIS and the AMSR-E datasets show similar variations in polynya area (Preußner et al., 2019), it was suggested that the two datasets have a high spatial and temporal reliability. Although MODIS can provide data with a resolution higher than 1 km, it is hard to guarantee complete temporal and spatial observations due to the limits of clouds and the shortwave radiation of the sun.

As a result, detailed studies of spatial and temporal variations of polynyas in the East Siberian Sea and Chukchi Sea are very limited and quantitative comparisons of different atmospheric and oceanic impacts on the polynyas are few. Also unknown is how sensitive the different AMSR-E resolution types (6.25 km and 12.5 km) are for picking up polynya areas in the East Siberian Sea and Chukchi Sea. In other words, how will the different AMSR-E datasets influence the study of the dynamics of atmospheric and oceanic factors on the variation of polynyas? Previous studies have focused on polynya in the entire region of the East Siberian Sea and Chukchi Sea. What is the difference in atmospheric and oceanic factors impacts on the polynyas in the different subregions? These questions have not been addressed in previous studies. Therefore, to

understand the processes and driving mechanisms for polynyas in the East Siberian Sea and Chukchi Sea, this study focuses on monthly and interannual variations of polynyas and the impacts of wind stress and ocean heat transport on the polynyas in different locations. Differences in polynya areas based on different resolutions and algorithms of AMSR-E data are also discussed quantitatively.

2. Data and methods

2.1. AMSR-E data

The AMSR-E data cover the period from June 2002 to October 2011. Since this study focuses on the months when polynyas typically exist, only the AMSR-E data from January to April over the period 2003–2011 was used. The area of polynyas was calculated for four cases with two traditional threshold methods (sea ice concentration and thickness) and AMSR-E data at spatial resolutions of 6.25 km and 12.5 km. Cases based on the threshold method of sea ice concentration at spatial resolutions of 6.25 km and 12.5 km are referred to as 6.25 km-IC and 12.5 km-IC, and cases based on sea ice thickness at spatial resolutions of 6.25 km and 12.5 km are referred to as 6.25 km-h and 12.5 km-h. For the sea ice concentration, a threshold of less than 75% is used to identify polynya (Massom et al., 1998). For the sea ice thickness, a value less than 0.2 m is often used as the polynya criterion (Preußner et al., 2019).

With respect to sea ice concentration, the 6.25 km-IC for 2003–2011 is based on the 6.25-km AMSR-E data product retrieved by Bremen University, Germany, and 12.5 km-IC is based on the 12.5-km AMSR-E data from the National Snow and Ice Data Center. For the sea ice thickness, the 6.25 km-h and 12.5 km-h for 2003–2011 were collected from the AMSR-E brightness temperature data of sea ice and derived through the algorithm developed for AMSR-E by Iwamoto et al. (2014).

The study region was divided into six small subregions (hereafter referred to as domains A, B, C, D, E, and F) based on the occurrence frequency of polynya. The frequency was calculated using the 6.25 km-IC along with the orientation and shape of the Siberian coast in the East Siberian Sea and Chukchi Sea from January through April over the period 2003–2011 (Fig. 1).

2.2. Wind data

The 10-m horizontal daily mean wind data for 2003–2011 (with spatial resolution of $0.25^\circ \times 0.25^\circ$) obtained from the European Center for Medium-Range Weather Forecasts (ECMWF) ERA5 were used to explore the impact of wind stress on polynyas in the six subregions of the East Siberian Sea and Chukchi Sea.

2.3. Ocean heat transport data

Simulated data for ocean heat transport for 2003–2011 were obtained from the Arctic Ocean unstructured-grid, Finite-Volume Community Ocean Model (AO-FVCOM). AO-FVCOM is a global-regional nested model driven by wind stress, sea level pressure, net heat flux, precipitation, evaporation and river discharge. The AO-FVCOM uses the ice-ocean coupled module based on the Community Ice Code (CICE), which was converted to the Unstructured Grid version (Hunke et al., 2010; Gao et al., 2011). AO-FVCOM has a horizontal resolution of 2–40 km (the higher resolution is in the regions with complex coastlines and topographies) and a vertical resolution derived using a hybrid terrain-following coordinate with 45 layers. No data assimilation was applied to the simulation. Detailed information about the model setup has been published in Chen et al. (2016), Zhang et al. (2016a), and Zhang et al. (2016b). The simulated results of AO-FVCOM have been validated under the climatological and real-time conditions for tidal

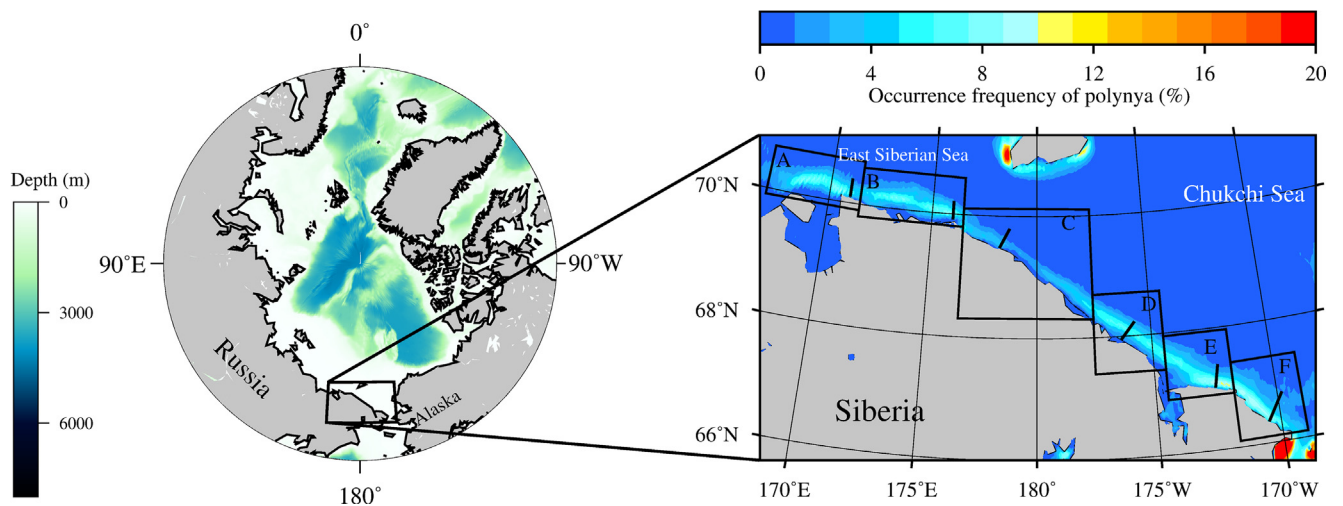


Fig. 1. The topography of the Arctic Ocean (left) and the occurrence frequency of polynya along the Siberian coast subregions in the East Siberian Sea and the Chukchi Sea from January to April over the period 2003–2011 (right). The black polygons indicate the six subregions and the black lines in the subregions indicate the transects used to calculate the ocean heat transport.

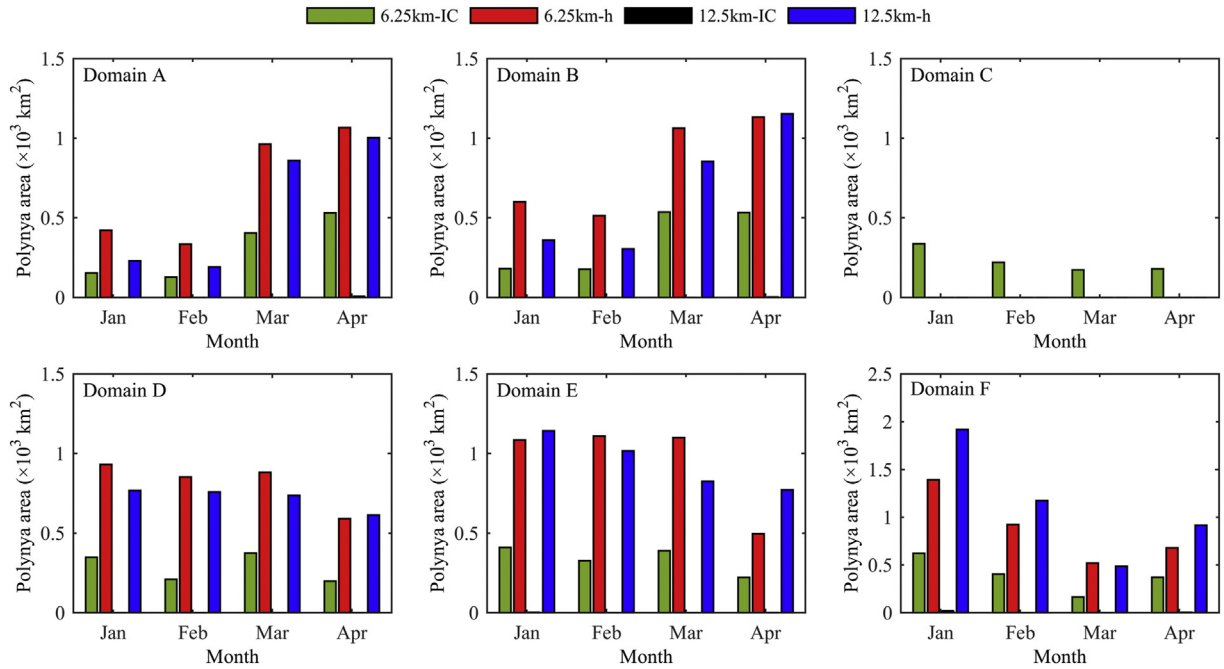


Fig. 2. The multi-year mean (2003–2011) monthly variation of polynya areas based on AMSR-E 6.25 km-IC, 6.25 km-h, 12.5 km-IC and 12.5 km-h in the six subregions from January to April.

elevation (Chen et al., 2009); current circulations (Chen et al., 2016); sea ice extent, concentration, thickness, and drift velocity (Gao et al., 2011; Zhang et al., 2016b); and water transports (Zhang et al., 2016a; Deng et al., 2019).

3. Monthly and interannual variations in polynya area

The monthly results showed that was hard to detect the polynyas in the case of 12.5 km-IC because most of the

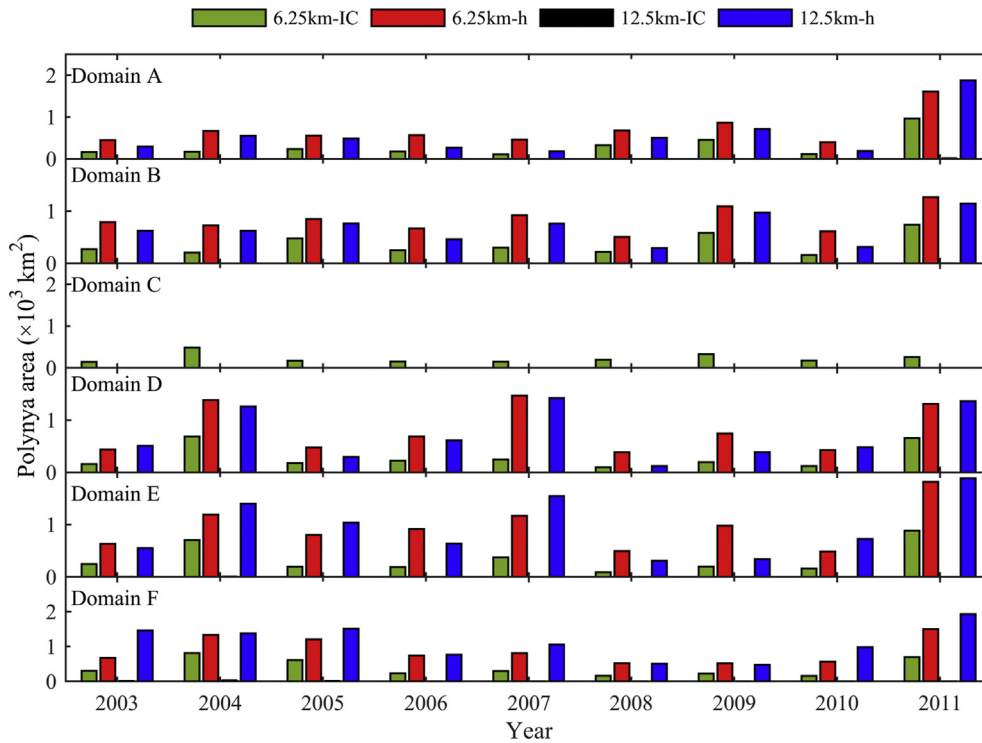


Fig. 3. The variation of annual (from January to April) polynya area based on AMSR-E 6.25 km-IC, 6.25 km-h, 12.5 km-IC and 12.5 km-h in the six subregions over the period 2003–2011.

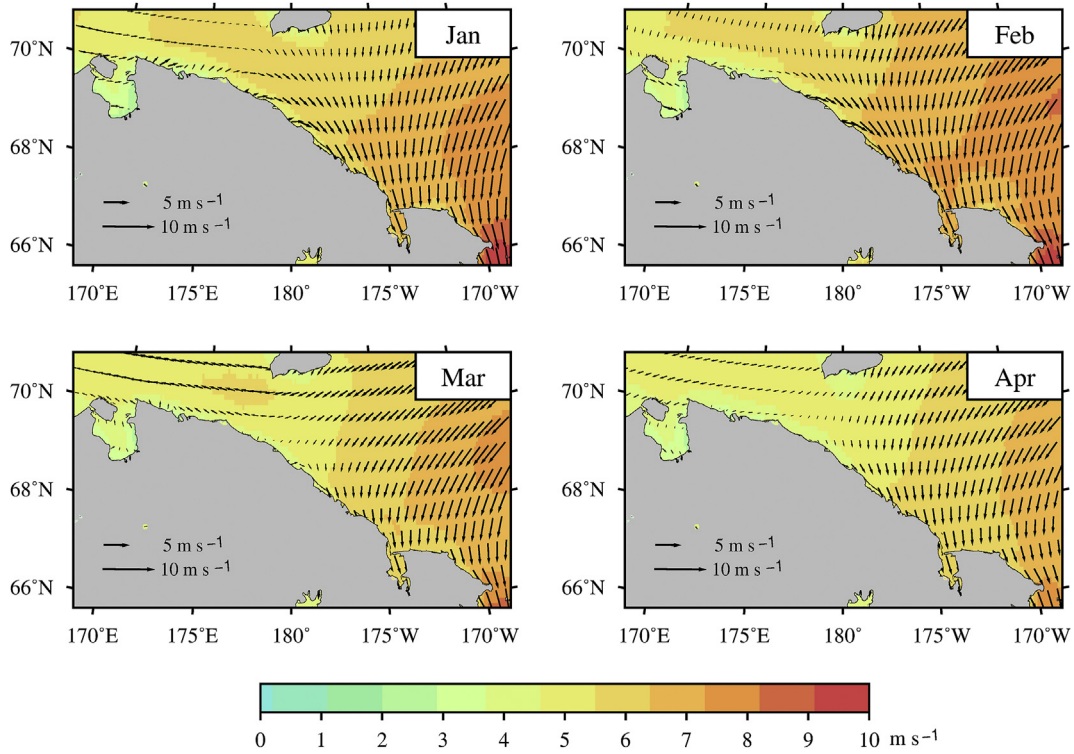


Fig. 4. The multi-year mean (2003–2011) monthly wind in the East Siberian Sea and Chukchi Sea from January to April.

derived sea ice concentration in the East Siberian Sea and Chukchi Sea were larger than 75 %, which resulted in a very small area of polynya in all of the subregions and periods. Therefore, in the following analysis and discussion, the 12.5 km-IC case was not included.

3.1. Monthly variation

The multi-year mean (2003–2011) monthly polynya areas from January to April showed large differences among the four cases (Fig. 2). For 6.25 km-IC, 6.25 km-h, and 12.5 km-h, the

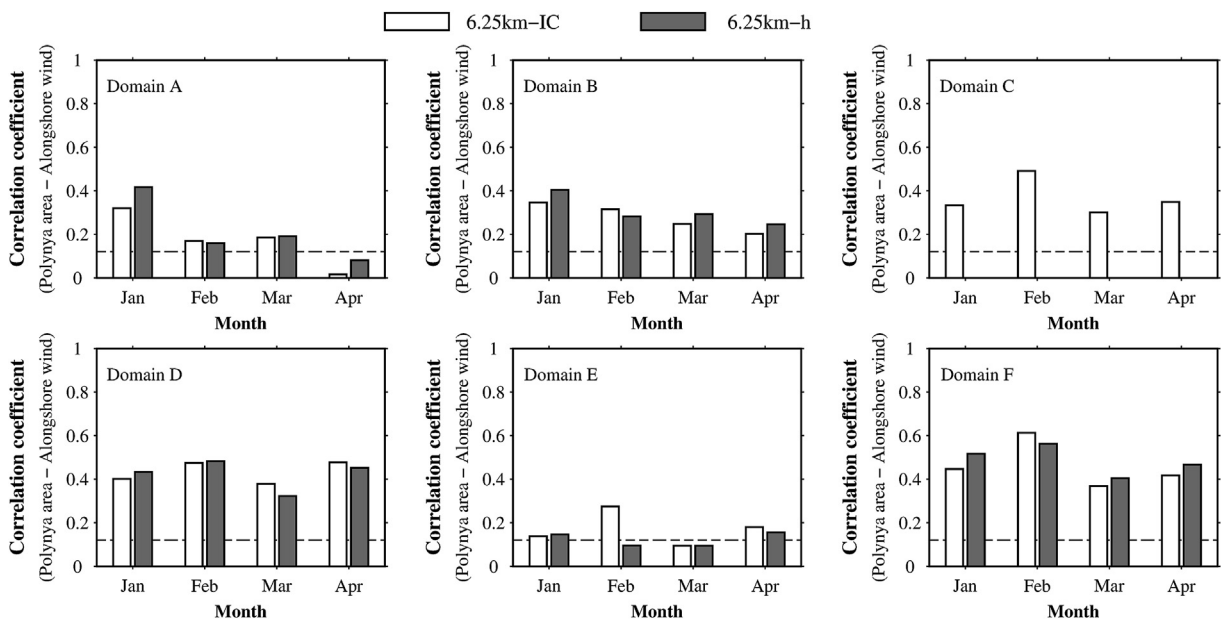


Fig. 5. The correlation coefficients between monthly alongshore wind speed and polynya area for the cases of 6.25 km-IC and 6.25 km-h in the six subregions from January to April over the period 2003–2011 (The dashed line indicates the 95 % confidence level).

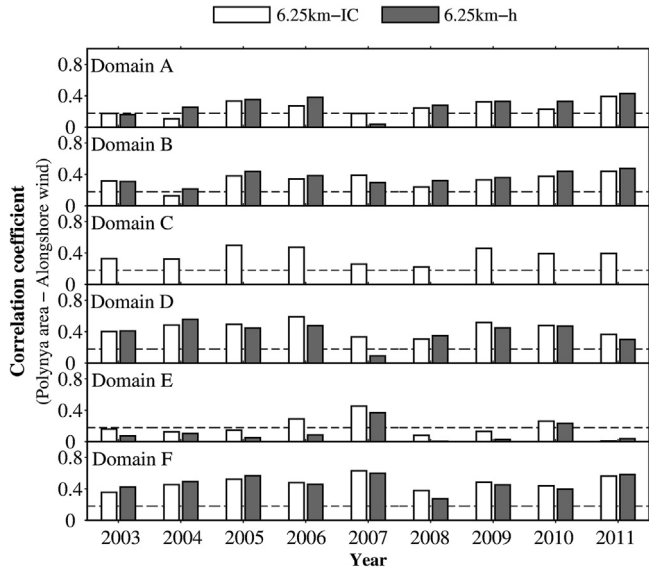


Fig. 6. The yearly (from January to April) correlation coefficients between alongshore wind speed and polynya area for the cases of 6.25 km-IC and 6.25 km-h in the six subregions over the period 2003–2011 (The dashed line indicates the 95 % confidence level).

maximum polynya areas in domains A and B occurred in April, while the maximum polynya area in domains D, E and F happened in January. In domain C, 6.25 km-h and 12.5 km-h could not detect polynya areas well, and only a small area of polynya was found in 6.25 km-IC. This suggests that domain C was dominated by sea ice with a large thickness and small concentration.

The cases using the sea ice thickness algorithm generated larger polynya areas than the cases using the sea ice concentration algorithm. However, they all reflected monthly variation of polynya area in each subregion (Fig. 2). The polynya areas in

6.25 km-h and 12.5 km-h were relatively similar whereas the cases of 6.25 km-IC and 6.25 km-h had the largest differences.

3.2. Interannual variation

The annual mean polynya area in each domain showed large interannual variation (Fig. 3). In domains A and B, the simulation results (except for 12.5 km-IC) showed a significantly larger polynya area in 2011. In domains D, E and F, the largest polynya areas appeared in 2004, 2007 and 2011. In domain C, the polynya areas for 6.25 km-h and 12.5 km-h were close to zero in all years. The polynya area for 6.25 km-IC was also smaller than in other domains.

4. Impacts of atmospheric and oceanic factors on polynya

The polynya areas in the four cases were quite different from one another due to differences in judgment methods and resolutions. In general, the higher resolution data captured a more detailed pattern of sea ice variation. The cases of 6.25 km-IC and 6.25 km-h were used to investigate the impacts of atmospheric and oceanic factors on the variation in polynya areas.

4.1. Impact of wind on polynya

During 2003–2011, northwest winds prevailed in the study area of the East Siberian Sea and Chukchi Sea from January to April (Fig. 4). The distribution pattern of wind speed in the four months was similar, increasing gradually from west to east with maximums close to Bering Strait. The mean wind speeds were larger in February and smaller in April.

The correlation between monthly alongshore wind speed and the polynya area for 6.25 km-IC and 6.25 km-h is shown in

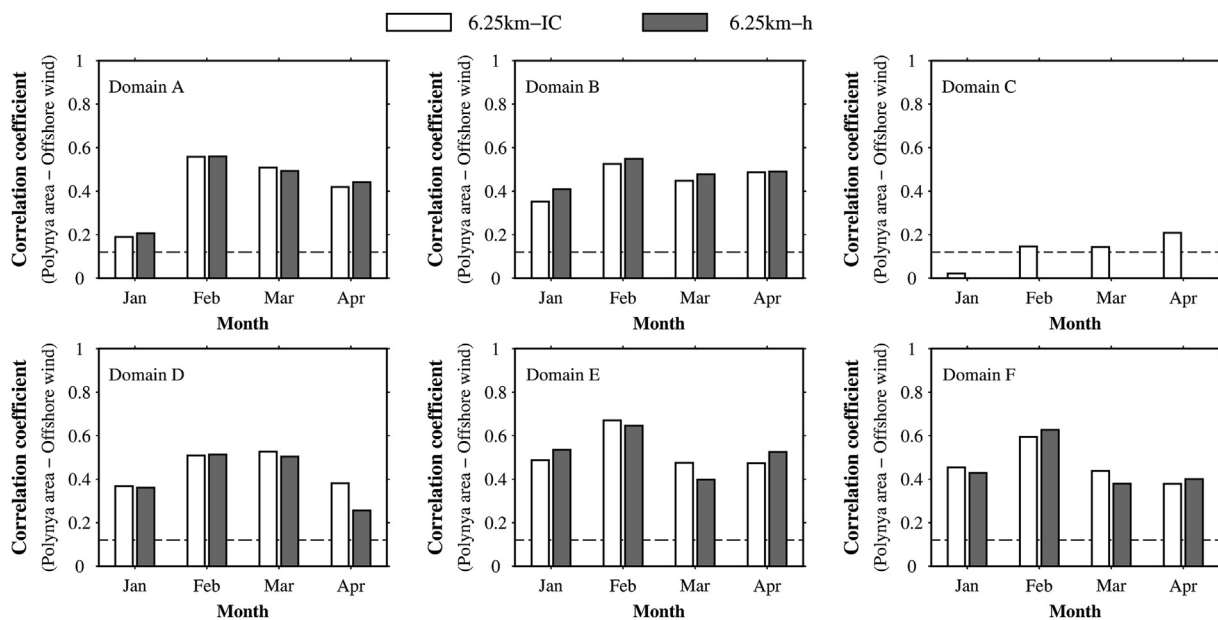


Fig. 7. The correlation coefficients between monthly offshore wind speed and polynya area for the cases of 6.25 km-IC and 6.25 km-h in the six subregions from January to April over the period 2003–2011 (The dashed line indicates the 95 % confidence level).

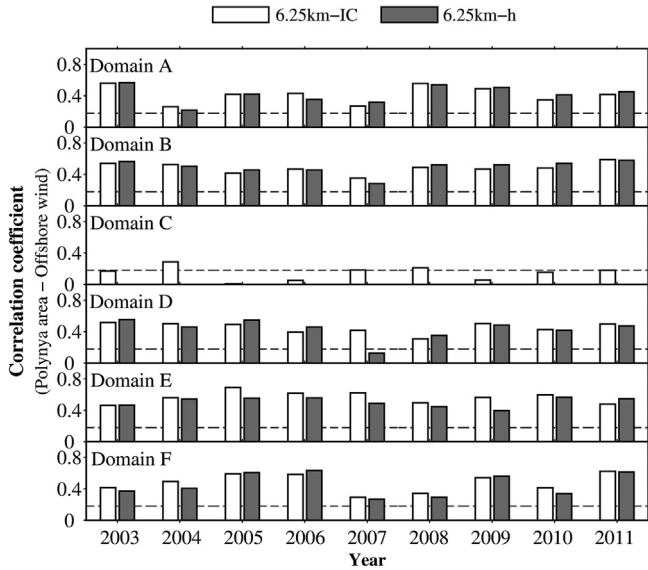


Fig. 8. The correlation coefficients between yearly (from January to April) offshore wind speed and polynya area for the cases of 6.25 km-IC and 6.25 km-h in the six subregions over the period 2003–2011 (The dashed line indicates the 95 % confidence level).

Fig. 5. Although the polynya area for 6.25 km-IC was very different from that of 6.25 km-h, the correlation between alongshore wind speed and the polynya area for these two cases had similar results (except in domain C). Both cases indicate that the alongshore wind had significant impacts on the polynya area. In domains D and F, the correlation coefficient was 0.43–0.47 at 95 % confidence level. In domain C, the 6.25 km-IC had a higher correlation with alongshore wind speed with the mean coefficient of 0.37. The 6.25 km-h could not detect any

polynya areas in domain C. In domains A and B, the 6.25 km-h showed a large correlation coefficient (over 0.40) in January.

The yearly correlation (from January to April) between alongshore wind speed and polynya area also showed small differences between the two cases and both with larger values (0.42–0.47) in domains D and F (Fig. 6). In each domain, a large amount of variability in the coefficient values was observed over the years. In domains A and B, both cases had maximum correlation coefficients in 2011. In domain C, the 6.25 km-IC had a maximum coefficient in 2005. In domain D, 6.25 km-IC and 6.25 km-h showed maximum values in 2006 and 2004, respectively. In domains E and F, the two cases had the maximum correlation coefficients in 2007.

The monthly correlation between offshore wind speed and the polynya area had larger coefficients than alongshore wind (Fig. 7). Both cases found that the offshore wind affected the polynya area significantly in every subregion except domain C. The smaller correlation coefficient in domain C was caused by the smaller polynya area.

Other domains had larger correlation coefficients but different patterns in different months. In domains A, B, E, and F, the maximum correlation coefficient appeared in February. In domain D, the correlation coefficient was almost the same in February and March. The month with the smallest correlation coefficient varied: January in domains A and B, March in domain E, and April in domains D and F.

In all domains except for domain C, the yearly (from January to April) correlation coefficient between offshore wind speed and polynya area was larger than with the alongshore wind (Fig. 8). The difference in correlation coefficients between these two cases was small. A maximum correlation coefficient of 0.69 occurred in 2005 for domain E. In domains A and D, the maximum

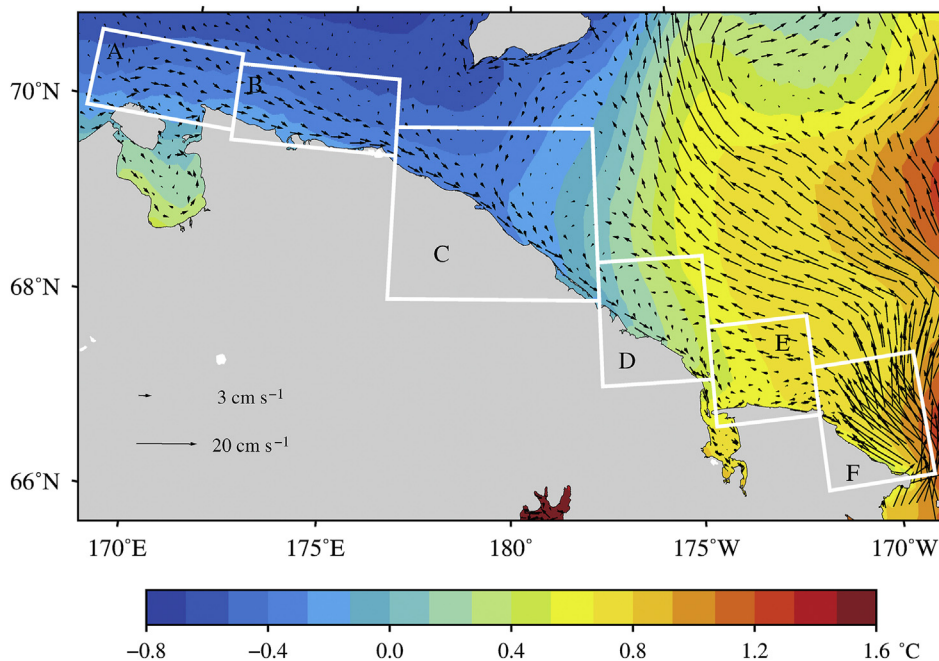


Fig. 9. The mean current and temperature of upper 10 m from January to April over the period 2003–2011.

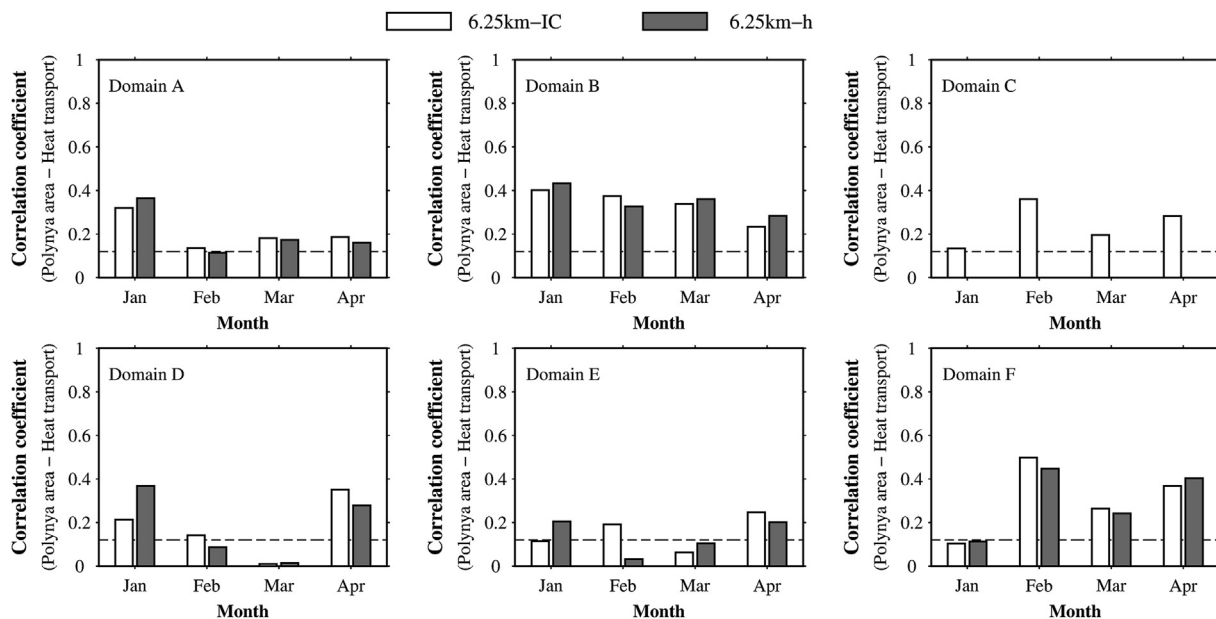


Fig. 10. The correlation coefficients between monthly ocean heat transport and polynya area for the cases of 6.25 km-IC and 6.25 km-h in the six subregions from January to April over the period 2003–2011. The dashed line indicates the 95 % confidence level.

correlation coefficient appeared in 2003. The maximum correlation value in domains B and F occurred in 2011.

4.2. Impact of ocean heat transport on polynya

The study area is a transitional zone between the Pacific-derived waters and the Arctic shelf waters with two currents that run in opposite directions (Semiletov et al., 2005) which was captured by our simulation (Fig. 9). Sensible heat polynyas in this area are thermally driven. The current circulation carries ocean heat into the study area and results in the continuous transport of warm water rising to the surface. Because of the shallow depth in the coastal region, sea ice is significantly affected by the surface layer water. Ocean heat transport in the upper 10 m in each subregion was calculated for the transects shown in Fig. 1. The transect location for each domain was selected based on the locations with the highest occurrences of polynya.

Fig. 10 shows the correlation between monthly ocean heat transport and the polynya area for 6.25 km-IC and 6.25 km-h. In general, the correlation coefficients for the two cases were similar. However, the correlation coefficient between ocean heat transport and polynya area was smaller than that between wind and polynya area, which suggests that the contribution of ocean heat transport to the polynya was not as significant as the contribution of the wind. Domain C was still a special case, without correlation values for 6.25 km-h. Compared with other domains, domains B and F had relatively larger correlation coefficients. Domains A and B had maximum correlation coefficients in January, and domain F had a maximum correlation value in February. In domains D and E, the maximum correlation for 6.25 km-IC was in April, while the maximum correlation for 6.25 km-h was in January.

The correlation coefficients between yearly ocean heat transport and polynya area for 6.25 km-IC and 6.25 km-h are shown in Fig. 11. Except for in domain C, there were small differences in correlation coefficients between 6.25 km-IC and 6.25 km-h. However, the correlation coefficients changed remarkably with the years and domains. Similar to the monthly result in Fig. 10, domains B and F had relatively larger correlation values (Fig. 11). In domain A, the largest correlation coefficient appeared in 2004 and 2006. In domains D and E,

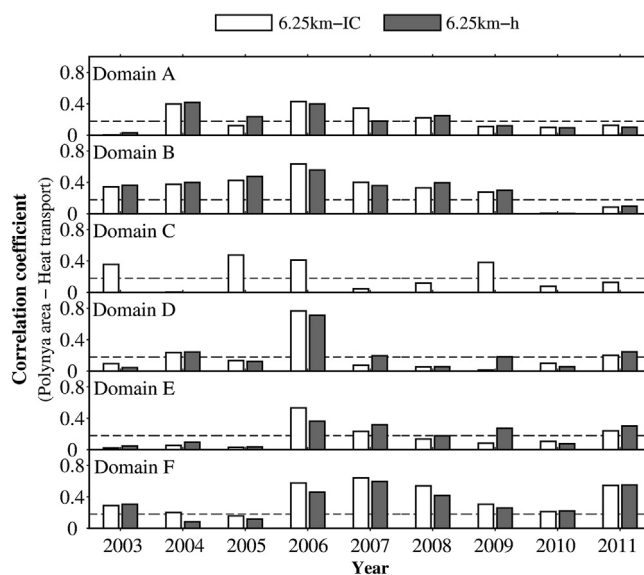


Fig. 11. The yearly (from January to April) correlation coefficients between ocean heat transport and polynya area for the cases of 6.25 km-IC and 6.25 km-h in the six subregions over the period 2003–2011 (The dashed line indicates the 95 % confidence level).

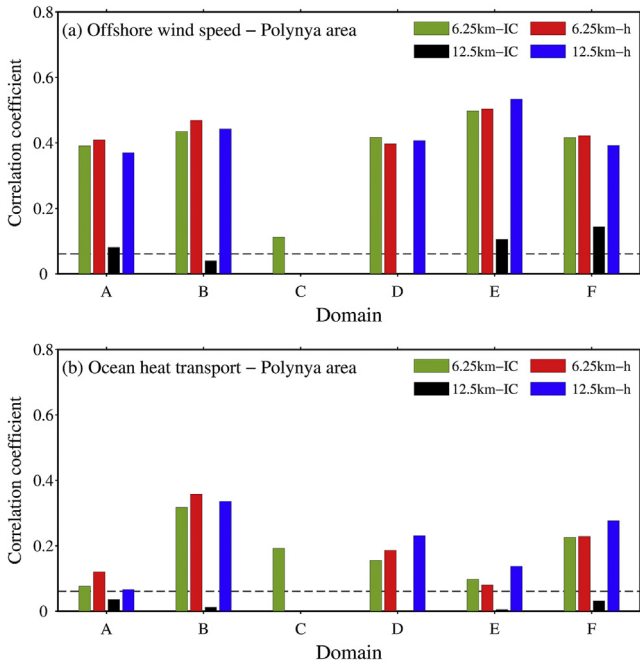


Fig. 12. The mean correlation coefficient between offshore wind speed and polynya area (a) and between ocean heat transport and polynya area (b) based on four cases of 6.25 km-IC, 6.25 km-h, 12.5 km-IC and 12.5 km-h in the six domains (2003–2011).

the maximum coefficient appeared in 2006 and was much larger than in other years.

5. Discussion

In the above analysis, only the higher resolution (6.25 km) AMSR-E dataset was used to explore the impacts of atmospheric and oceanic factors on polynya in the East Siberian Sea

and Chukchi Sea. Further correlation analysis was conducted and discussed using the relatively coarse resolution of 12.5 km. There were large differences between the results for 12.5 km-IC and the results for the other three cases in that it was hard to detect polynyas in 12.5 km-IC (Fig. 12).

With respect to the correlation between offshore wind speed and polynya area, the three cases of 6.25 km-IC, 6.25 km-h and 12.5 km-h showed similar trends with the maximum coefficients appearing in domain E. The correlation between ocean heat transport and polynya area had the same pattern except that the maxima occurred in domain B. The only difference among these three cases was that it was hard to detect the polynya in domain C with either 6.25 km-h or 12.5 km-h. For the study of the correlations between polynya area and atmospheric and oceanic factors in the East Siberian Sea and Chukchi Sea, the higher resolution dataset is strongly recommended although the coarser resolution of 12.5 km for AMSR-E dataset can be used with the algorithm of sea ice thickness.

In the analysis of the correlation between wind speed and polynya area, the correlation coefficients were large. However, the wind velocity characteristics across the five domains were different, which influenced the polynya area in different ways. Wind direction also played a role in the formation of polynya. In domains A and B in the East Siberian Sea, the east–west winds (which roughly parallel the Siberian coast) accounted for 70.8 % and 75.4 % respectively (Fig. 13). This wind direction in domains A and B was helpful in the formation of polynya in that the wind could cause the sea ice to drift along the coast. In domains D, E and F of the Chukchi Sea, most of the wind was northwest but the wind speed was greater than that in domains A and B (mean values of 5.6 m s⁻¹ for domain D, 5.7 m s⁻¹ for domain E and 6.0 m s⁻¹ for domain F) (Fig. 13). The stronger winds in domains D, E and F still could produce the relatively large along-coast wind component

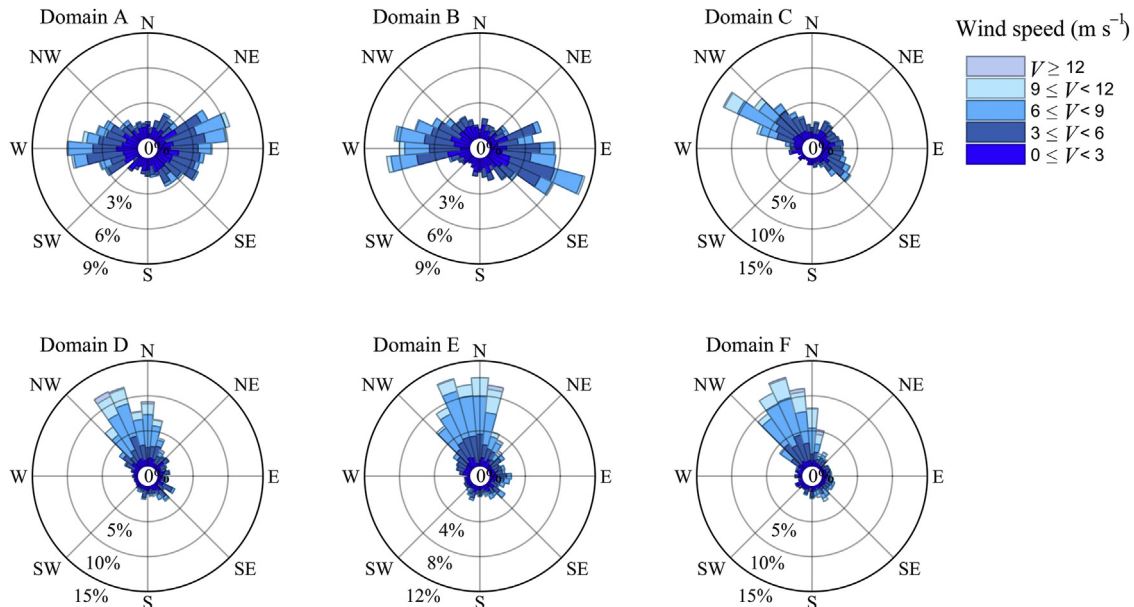


Fig. 13. The percentage distributions of wind speed and direction in the six domains over the period 2003–2011.

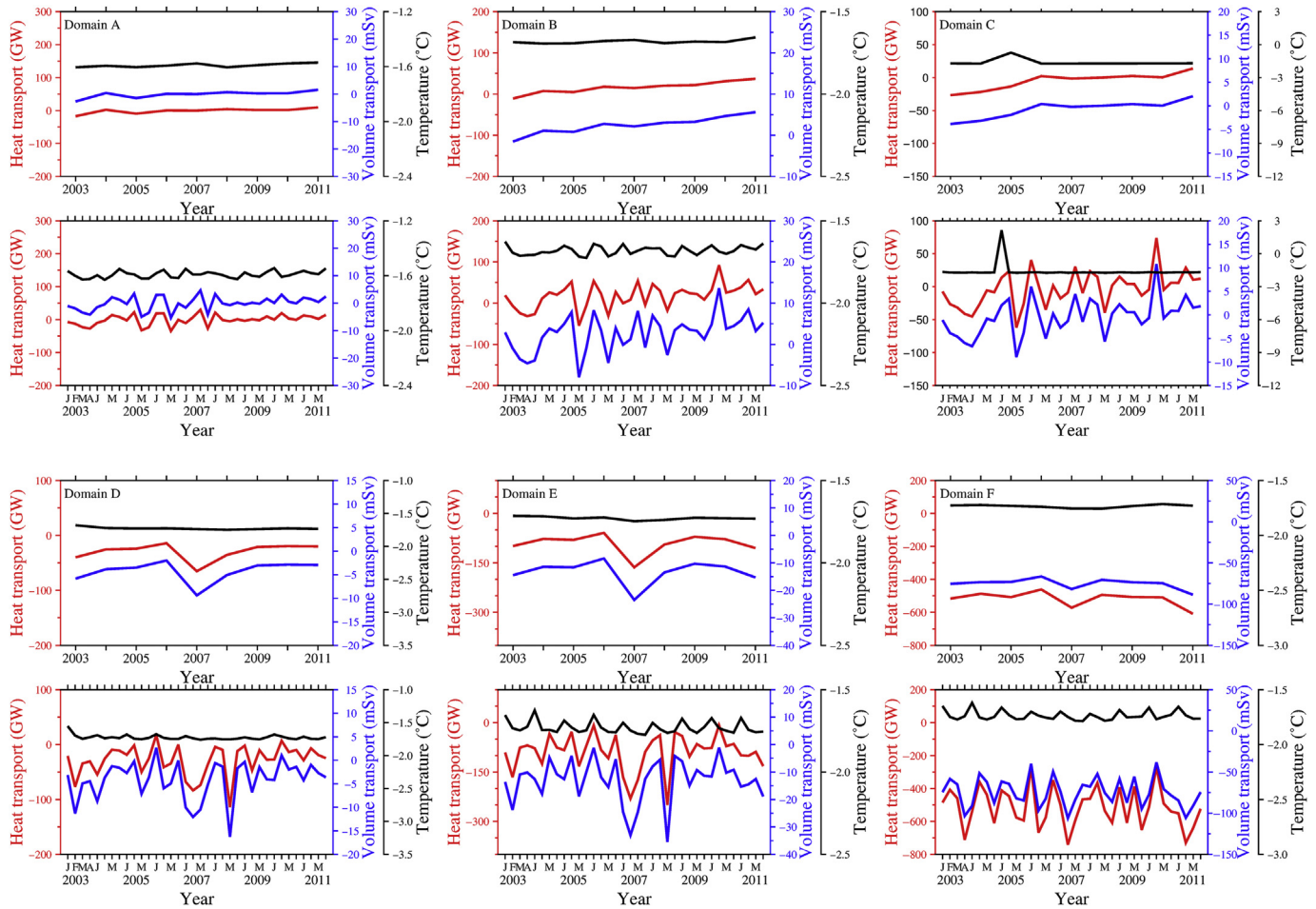


Fig. 14. Comparisons of yearly (top) and monthly (bottom) ocean heat transport, volume transport, and temperature in the upper 10 m in the six domains from January to April over the period 2003–2011 (The negative values in the volume transport indicate the current flowing from the East Siberian Sea to the Chukchi Sea, and the positive values indicate the opposite direction).

affecting the sea ice movement. We believe that wind direction dominates the formation of polynya in the East Siberian Sea and wind speed dominates the formation of polynya in the Chukchi Sea.

In the study of the influence of ocean heat transport on polynya, the roles of variation of water temperature and volume transport in heat transport were explored since the heat transport was determined by the water temperature and water velocity. Comparisons of yearly and monthly ocean heat transport, volume transport and temperature in the upper 10 m showed that variations in volume transport were highly correlated ($r > 0.9$, $p < 0.01$) with variations in heat transport (Fig. 14). Variations in water temperature had a very low correlation ($r < 0.1$) with variations in heat transport. This result indicates that the heat transport in the East Siberian Sea and Chukchi Sea was dominant by volume transport during the study period.

6. Conclusions

Multi-year mean monthly and annual simulations of polynya area showed distinct differences among the study domains. In general, 6.25 km-h and 12.5 km-h derived larger polynya areas than 6.25 km-IC and 12.5 km-IC. The exception

is domain C, where no polynya could be detected with 6.25 km-h and 12.5 km-h because the sea ice thickness in these two cases was larger than the polynya criterion of 0.2 m. The case of 12.5 km-IC showed sea ice concentration larger than 75 %, which made it difficult to detect the polynyas in all the domains. In general, the difference in polynya area between 6.25 km-h and 12.5 km-h was larger than the difference in polynya area between 6.25 km-IC and 12.5 km-IC.

Both the alongshore and offshore winds affected variation in the polynyas. The correlation coefficient between wind speed and polynya area was larger than that between ocean heat transport and polynya area, which suggests a smaller contribution of ocean heat transport to the polynya area than the contribution of wind.

The difference in correlation between results for 12.5 km-h and 6.25 km-h is smaller. AMSR-E sea ice thickness data with a coarse resolution of 12.5 km can be used for the study of atmospheric and oceanic mechanisms on polynya area, but the higher resolution dataset is suggested as the first choice.

Both wind direction and wind speed were important factors affecting the polynya. Wind direction dominated the polynya area in the East Siberian Sea and wind speed was dominant in the Chukchi Sea. Variations in ocean heat transport in the East

Siberian Sea and Chukchi Sea was controlled by variations in volume transport rather than by variations in water temperature.

Declaration of competing interest

The authors declare no conflict of interests.

Acknowledgment

This work was supported by the National Key Research and Development Program of China (2019YFA0607000) and the National Natural Science Foundation of China (41706210) for Yu Zhang, the Innovation Group Project of Southern Marine Science and Engineering Guangdong Laboratory (Zhuhai) (311021009) for Dan-Ya Xu, the U.S. National Science Foundation (PLR-1603000) for Chang-Sheng Chen and Shanghai Pujiang Program (19PJ1404300) for Liang Chang. The development of the AO-FVCOM was also supported by the International Center for Marine Studies (ICMS) at the Shanghai Ocean University (SHOU). The simulation was conducted on the super performance Linux cluster in SHOU and we thank our SHOU collaborators for their efforts in the maintenance of the cluster for this research.

References

- Barber, D., Marsden, R., Minnett, P., et al., 2001. Physical processes within the north water (NOW) polynya. *Atmos.-Ocean* 39, 163–166.
- Bi, H., Liang, Y., Wang, Y., et al., 2020. Arctic multiyear sea ice variability observed from satellites: a review. *J. Ocean. Limnol.* 38, 962–984.
- Chen, C., Gao, G., Qi, J., et al., 2009. A new high-resolution unstructured grid finite volume Arctic Ocean model (AO-FVCOM): an application for tidal studies. *J. Geophys. Res. Oceans* 114, C08017. <https://doi.org/10.1029/2008JC004941>.
- Chen, C., Gao, G., Zhang, Y., et al., 2016. Circulation in the Arctic Ocean: results from a high-resolution coupled ice-sea nested Global-FVOM and Arctic-FVCOM system. *Prog. Oceanogr.* 141, 60–80.
- Comiso, J.C., 2006. Arctic warming signals from satellite observations. *Weather* 61 (3), 70–76.
- Comiso, J.C., 2012. Large decadal decline of the Arctic multiyear ice cover. *J. Clim.* 25 (4), 1176–1193.
- Danielson, S.L., Weingartner, T.J., Hedstrom, K.S., et al., 2014. Coupled wind-forced controls of the Bering–Chukchi shelf circulation and the Bering Strait throughflow: Ekman transport, continental shelf waves, and variations of the Pacific–Arctic sea surface height gradient. *Prog. Oceanogr.* 125, 40–61.
- Deng, Y., Gao, G., Zhang, Y., et al., 2019. Seasonal and interannual variability of Bering Strait throughflow from AO-FVCOM and observation. *J. Ocean Univ. China* 18 (3), 615–625.
- Durski, S.M., Kurapov, A.L., 2020. A high-resolution coupled ice–ocean model of winter circulation on the Bering Sea Shelf. Part II: polynyas and the shelf salinity distribution. *Ocean Model.* 156. <https://doi.org/10.1016/j.ocemod.2020.101696>.
- Fukamachi, Y., Simizu, D., Ohshima, K.I., et al., 2017. Sea-ice thickness in the coastal northeastern Chukchi Sea from moored ice-profiling sonar. *J. Glaciol.* 63 (241), 888–898.
- Gao, G., Chen, C., Qi, J., et al., 2011. An unstructured-grid, finite-volume sea ice model: development, validation, and application. *J. Geophys. Res. Oceans* 116, C00D04. <https://doi.org/10.1029/2010JC006688>.
- Grebmeier, J.M., Cooper, L.W., 1995. Influence of the St. Lawrence island polynya upon the Bering Sea benthos. *J. Geophys. Res.* 100 (C3), 4439–4460.
- Häkkinen, S., 1993. An Arctic source for the great salinity anomaly: a simulation of the Arctic ice–ocean system for 1955–1975. *J. Geophys. Res. Oceans* 98, 16397–16410.
- Hall, A., 2004. The role of surface albedo feedback in climate. *J. Clim.* 17 (7), 1550–1568.
- Hirano, D., Fukamachi, Y., Watanabe, E., et al., 2016. A wind-driven, hybrid latent and sensible heat coastal polynya off Barrow, Alaska. *J. Geophys. Res. Oceans* 121, 980–997.
- Hunke, E.C., Lipscomb, W.H., Turner, A.K., 2010. CICE: the Los Alamos Sea Ice Model documentation and software User's Manual, Version 4.1, Tech. Rep. LA-CC-06-012. Los Alamos Natl. Lab.
- Ingram, R.G., Bâcle, J., Barber, D.G., et al., 2002. An overview of physical processes in the North Water. *Deep-Sea Res. Pt II* 49, 4893–4906.
- Iwamoto, K., Ohshima, K.I., Tamura, T., 2014. Improved mapping of sea ice production in the Arctic Ocean using AMSR-E thin ice thickness algorithm. *J. Geophys. Res. Oceans* 3574–3594.
- Johannessen, O.M., Bengtsson, L., Miles, M.W., et al., 2004. Arctic climate change: observed and modelled temperature and sea-ice variability. *Tellus* 56 (4), 328–341.
- Kottmeier, C., Engelbart, D., 1992. Generation and atmospheric heat-exchange of coastal polynyas in the Weddell Sea. *Bound-Lay. Meteorol.* 60, 207–234.
- Kozo, T.L., 1991. The hybrid polynya at the northern end of Nares Strait. *Geophys. Res. Lett.* 18, 2059–2062.
- Kwok, R., Rothrock, D.A., 2009. Decline in Arctic sea ice thickness from submarine and ICESat records: 1958–2008. *Geophys. Res. Lett.* 36 (15). <https://doi.org/10.1029/2009GL039035>.
- Kwok, R., Cunningham, G.F., Wensnahan, M., et al., 2009. Thinning and volume loss of the Arctic Ocean sea ice cover: 2003–2008. *J. Geophys. Res. Oceans* 114 (C7). <https://doi.org/10.1029/2009JC005312>.
- Ladd, C., Mordy, C.W., Salo, S.A., et al., 2016. Winter water properties and the Chukchi polynya. *J. Geophys. Res. Oceans* 121, 5516–5534.
- Lei, R., Xie, H., Wang, J., et al., 2015. Changes in sea ice conditions along the Arctic Northeast Passage from 1979 to 2012. *Cold Reg. Sci. Technol.* 119, 132–144.
- Liang, X., Losch, M., 2018. On the effects of increased vertical mixing on the Arctic Ocean and sea ice. *J. Geophys. Res. Oceans* 123 (12), 9266–9282.
- Lytle, V.I., Ackley, S.F., 1996. Heat flux through sea ice in the western Weddell Sea: convective and conductive transfer processes. *J. Geophys. Res. Oceans* 101, 8853–8868.
- Martin, S., Cavalieri, D.J., 1989. Contributions of the Siberian shelf polynyas to the Arctic Ocean intermediate and deep water. *J. Geophys. Res.* 94, 12725–12738.
- Massom, R.A., Harris, P.T., Michael, K.J., et al., 1998. The distribution and formative processes of latent-heat polynyas in East Antarctica. *Ann. Glaciol.* 27, 420–426.
- Maykut, G.A., 1982. Large-scale heat exchange and ice production in the central Arctic. *J. Geophys. Res.* 87 (C10), 7910–7984.
- Maykut, G.A., McPhee, M.G., 1995. Solar heating of the Arctic mixed layer. *J. Geophys. Res. Oceans* 100, 24691–24703.
- McPhee, M.G., Stanton, T.P., Morison, J.H., et al., 1998. Freshening of the upper ocean in the Arctic: is perennial sea ice disappearing? *Geophys. Res. Lett.* 25 (10), 1729–1732.
- Melling, H., Haas, C., Brossier, E., 2015. Invisible polynyas: modulation of fast ice thickness by ocean heat flux on the Canadian polar shelf. *J. Geophys. Res. Oceans* 120, 777–795.
- Morales Maqueda, M.A., Willmott, A.J., Biggs, N.R.T., et al., 2004. Polynya dynamics: a review of observations and modeling. *Rev. Geophys.* 42, RG1004. <https://doi.org/10.1029/2002RG000116>.
- Perovich, D.K., Light, B., Eicken, H., et al., 2007. Increasing solar heating of the Arctic Ocean and adjacent seas, 1979–2005: attribution and role in the ice-albedo feedback. *Geophys. Res. Lett.* 34 (19). <https://doi.org/10.1029/2007GL031480>.
- Pisareva, M.N., Pickart, R.S., Lin, P., et al., 2019. On the nature of wind-forced upwelling in Barrow Canyon. *Deep-Sea Res. Pt II* 162, 63–78.
- P्रेुßer, A., Ohshima, K.I., Iwamoto, K., et al., 2019. Retrieval of wintertime sea ice production in Arctic polynyas using thermal infrared and passive microwave remote sensing data. *J. Geophys. Res. Oceans* 124, 5503–5528.

- Rothrock, D.A., Yu, Y., Maykut, G.A., 1999. Thinning of the Arctic sea-ice cover. *Geophys. Res. Lett.* 26 (23), 3469–3472.
- Schauer, U., 1995. The release of brine enriched shelf water from Storfjord into the Norwegian sea. *J. Geophys. Res.* 100, 16015–16028.
- Screen, J.A., Simmonds, I., 2010. The central role of diminishing sea ice in recent Arctic temperature amplification. *Nature* 464 (7293), 1334–1337. <https://doi.org/10.1038/nature09051>.
- Semiletov, I., Dudarev, O., Luchin, V., et al., 2005. The East Siberian Sea as a transition zone between Pacific-derived waters and Arctic shelf waters. *Geophys. Res. Lett.* 32 <https://doi.org/10.1029/2005GL022490>.
- Stroeve, J., Holland, M.M., Meier, W., et al., 2007. Arctic sea ice decline: faster than forecast. *Geophys. Res. Lett.* 34 (9). <https://doi.org/10.1029/2007GL029703>.
- Sturm, M., Perovich, D.K., Holmgren, J., 2002. Thermal conductivity and heat transfer through the snow on the ice of the Beaufort Sea. *J. Geophys. Res. Oceans* 107. <https://doi.org/10.1029/2000JC000409>.
- Vincent, R.F., 2019. A study of the North Water Polynya ice arch using four decades of satellite data. *Sci. Rep.* 9. <https://doi.org/10.1038/s41598-019-56780-6>.
- Vincent, R.F., 2020. An examination of the non-formation of the North Water Polynya ice arch. *Rem. Sens.* 12 (17). <https://doi.org/10.3390/rs12172712>.
- Winsor, P., Björk, G., 2000. Polynya activity in the Arctic Ocean from 1958–1997. *J. Geophys. Res.* 105, 8789–8803.
- Woodgate, R.A., Aagaard, K., Weingartner, T.J., 2005. Monthly temperature, salinity, and transport variability of the Bering Strait through flow. *Geophys. Res. Lett.* 32 (4) <https://doi.org/10.1029/2004GL021880>.
- Yamamoto-Kawai, M., McLaughlin, F.A., Carmack, E.C., et al., 2008. Freshwater budget of the Canada basin, Arctic Ocean, from salinity, $\delta^{18}\text{O}$, and nutrients. *J. Geophys. Res. Oceans* 113. <https://doi.org/10.1029/2006JC003858>.
- Zhang, Y., Chen, C., Beardsley, R.C., et al., 2016a. Seasonal and interannual variability of the Arctic sea ice: a comparison between AO-FVCOM and observations. *J. Geophys. Res. Oceans* 121 (11), 8320–8350.
- Zhang, Y., Chen, C., Beardsley, R.C., et al., 2016b. Studies of the Canadian Arctic Archipelago water transport and its relationship to basin-local forcings: results from AO-FVCOM. *J. Geophys. Res. Oceans* 121 (6), 4392–4415.